Photon-Migration Measurement of Latex Size Distribution in Concentrated Suspensions

Eva Sevick-Muraca, Joseph Pierce, Huabei Jiang, and Jeffrey Kao
School of Chemical Engineering, Purdue University, West Lafayette, IN 47907

Frequency-domain measurements of photon migration were conducted in concentrated polystyrene suspensions to assess their use for on-line particle sizing in undiluted process streams. Using a numerical inverse algorithm, particle-size distributions (PSD) and volume fractions of three latex suspensions with differing distributions were recovered from phase-shift measurements at 15 or less visible wavelengths. Comparison to dynamic light-scattering measurements show excellent agreement. Since it is the propagation characteristics of multiply scattered light instead of the amount of light detected that is employed to solve the inverse problem, the measurement technique provides a self-calibrating (and therefore especially suitable) method for on-line process monitoring of PSD in the chemical-based industries.

Introduction

The optimization and control of particulate and dispersed phase processes is especially difficult, since the critical process parameters of particle-, crystal-, or dispersed phase-size distributions (PSD, CSD, or DPSD) and their volume fractions currently escape on-line measurement. The errors associated with process sampling, the sample destruction prior to off-line analysis, and the long analysis times not only prevent real-time process measuring of these critical parameters, but also impede or prevent model verification and robust parameter identification for model-based control and optimization (for review see Dimitratos et al., 1994; Rawlings et al., 1993). For example, while population-balance models might predict PSD and CSD in emulsion polymerization and crystallization processes, they require parameter identification of nucleation, growth, coalescence, and breakup rates, each of which depends on the PSD, CSD, or DPSD in an unknown fashion. The inability to measure these unknown parameters causes significant problems in the formulation of nonlinear models for these processes. Consequently, the lack of accurate modeling of emulsion polymerization, crystallization, and liquid–liquid dispersion processes coupled with the lack of robust measurements have forced the use of open-loop control, based inefficiently upon measurements downstream and, in some cases, upon final product quality.

Correspondence concerning this article should be addressed to E. Sevick-Muraca.

Optical measurements of PSD, CSD and DPSD

Optical techniques offer opportunities for sensing particle-, crystal-, or dispersed-size distributions which, when combined with validated process models, may provide control and optimization for 70–80% of the chemical-based industry. Despite difficulties plaguing them, there are four particle-sizing approaches under development for on-line monitoring of PSD: (1) dynamic light scattering, (2) angular scattering measurements, (3) turbidity measurements, and (4) laser reflection measurements (see Figure 1).

Dynamic Light Scattering. Dynamic light scattering (DLS, also termed quasi-elastic light scattering or photon correlation spectroscopy) monitors the fluctuation of light intensity due to the Brownian motion of a single particle into and out of the near field. From the time-dependence of intensity fluctuations, the particle diffusion coefficient can be computed and the radius obtained from the Stokes–Einstein equation. A statistical number of measurements of diluted and pretreated samples can provide an accurate measure of PSDs of less than 10 microns (μm).

Angular Scattering Measurements. In contrast to the hydrodynamic measurement of DLS, these measurements monitor the angular scatter of light at a single wavelength due to diffraction from a single particle. Using classic scattering theory and known refractive indices of fluid and particle, an equivalent radius can be computed from an inverse solution. Again, a statistical number of measurements can provide accurate PSDs from diluted samples with diameters greater than 10 μm. Rawlings and coworkers (1993) report particle-size

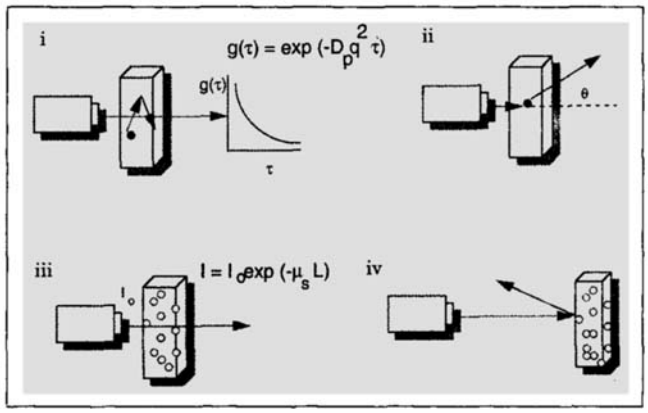

Figure 1. Optical techniques for on-line sensing of particle-size distributions.

(i) Dynamic light scattering, (ii) diffraction measurements, (iii) turbidity measurements, and (iv) laser reflection techniques.

reconstructions from classic scattering theory using simulated measurements for CSDs between 10 and 100 μm.

Turbidity Measurements. Tubidity (τ) measurements monitor the attenuation of light at multiple wavelengths at an angle of 180° from its incidence due to scatter in all directions out of the path length. Scattering occurs by either single particles or ensembles of particles. However, since backscatter or multiple scattering of light back into the path length is not accounted for, turbidity measurements must be conducted on diluted samples such that the product of turbidity, τ, and path length, L, is less than 0.3. In other words, the optical path of the sample is no less than three times the mean distance between scattering particles (Van de Hulst, 1983). Upon using classic scattering theories to compute $Q_{\text{scat}}(x, n, \lambda)$, or the scattering efficiency of spherical particles of diameter x and relative refractive index n, measurements of turbidity conducted at several wavelengths can be used to obtain PSDs, or $f(x)$ from solution to the inverse problem:

$$\tau(\lambda) = -\log \frac{I}{I_0} = \mu_s(\lambda) = \int_0^\infty \frac{3Q_{\text{scat}}(x, n, \lambda)}{2x} \phi f(x)\, dx, \quad (1)$$

where I_0 is the intensity of incident radiation; I is the intensity of measured radiation; ϕ is the unknown total volume fraction of particles; and $f(x)$ is the unknown particle-size distribution. Nonlinear least-squares determination of $f(x)$ has been successfully performed on simulated aerosol-size distributions from satellite sensors calibrated by use of the solar-occultation technique (Wang et al., 1996). Upon assuming bimodal log-normal aerosol distributions, size distributions in the range of 0.1–1.5 μm were recovered from seven simulated wavelength measurements. These authors also demonstrate that shape-constraint-free size distributions can be derived from simulated measurements. Upon discretizing Eq. 1 and employing regularization techniques to determine the discrete size fractions, $f(x)_i$, of particles with diameters between $x_i + \Delta x_i$, Elicabe and Garcia-Rubio (1990) have demonstrated reconstruction of unimodal and bimodal latex PSDs from simulated turbidimetric measurements of arbitrary-size distribution shapes from 701 wavelength measurements with a maximum value of random noise of 3%. Using similar techniques, Wang and coworkers (1996) show the ability to recover the PSD of a mixture of two monodisperse latexes of different diameters. Yet another set of investigators, Wang and Hallett (1996) have recently reconstructed a unimodal latex size distribution from experimental turbidity measurements using an analytical inversion method that also does not assume a distribution form. These authors unfortunately report neither the number of wavelengths employed nor the resolution of the discretized, reconstructed size fractions, $f(x)_i$. However, their result of a reconstructed latex size distribution shows that PSDs reconstructed from turbidity measurements underpredict large-size fractions in comparison to DLS measurements. Using turbidity measurements at five to eight wavelengths, Vavra and coworkers (1995) reconstructed the mean and variance of assumed log-normal distributions of LUDOX and PVC latex. Their numerical inversions are excellent for LUDOX, but poorly predict the variance of the latex distribution.

To improve the solution of the inverse problem, turbidity measurements have been combined with size-exclusion (Allen, 1990) and capillary-hydrodynamic (Silebi and Dos Ramos, 1989) chromatography separation techniques in order to provide relatively monodisperse, diluted suspensions for prediction of the number of particles, N_i, with diameter $x_i + \Delta x_i$ from attenuation measurements:

$$\tau_i(\lambda) = \mu_{s_i}(\lambda) = \frac{N_i Q_{\text{scat}}(x_i, n, \lambda) \pi x_i^2}{4}. \quad (2)$$

Advantages/Disadvantages to DLS, Diffraction, and Turbidity Measurements. Due likely to (1) the difficulties in calibrating the spectral response of the detector and lamp (which requires replacement on the average of every 1,000 h); (2) the potential changes in wavelength-dependent sample absorbance during normal process disturbances and changing feedstocks; and (3) the difficulties in sample dilution; reconstruction of particle sizes from experimental turbidity and diffraction measurements have yet to be consistently demonstrated.

Nonetheless, the implementation of DLS, diffraction, and turbidity each have been proposed using side or split streams in emulsion polymerization (Thomas et al., 1996; Kourti et al., 1990) and crystallization processes (Jager et al., 1992). Besides the difficulties associated with shear induced breakup of dispersed phase in on-line sample chambers, DLS and diffraction measurements require discrete, single-particle measurements and nontrivial automated sampling. For sizing liquid droplets, side-stream measurements induce coalescence and breakup. For sizing solids, side-stream measurements create maintenance problems such as clogged pumps, conduits, and filters. Turbidity can also require substantial dilution. Turbidity and diffraction or angular scattering measurements require calibration for changes in the suspending fluid absorbance.

Laser Reflection. Of the established techniques, *backscatter* or *laser reflection measurements* offer an attractive opportunity for on-line sensing of particle-size distribution in suspensions ranging from 0.01% to 30% by volume. The technique consists of monitoring the reflection of spatially rotating laser light as particles pass through the focal point of the

optical-sensor head. The back-reflected light is collected and assumed to be proportional to the area of the particle. Assuming spherical particles, a particle-size determination is made. The technique requires calibration for the particulate and its suspending fluid and provides particle sizing of particulates located close to the sensor within the range of 10–1,000 μm. Typically, backscatter techniques overestimate submicron particles sizes (Sparks and Dobbs, 1993) and underestimate large ones (Monnier et al., 1996). Similar to DLS and diffraction measurements, laser reflection techniques are based on discrete single-particle measurements to reconstruct PSD. Laser reflection measurements are sensitive to erroneous positioning of the focal plane, contribution of higher-order scattering, and sampling error brought about by the hydrodynamic partitioning of large particles away from the wall and sensor head. In addition, the measurements are reported not to be accurate with nonopaque particles or dispersed droplets (Sparks and Dobbs, 1993). Nonetheless, Farrell and Tsai (1995) report laser reflection sensing for control of potassium sulfate crystallizers.

Summary of Methods. None of the methods mentioned previously give a measurement of the particulate volume fraction of an undiluted, untreated sample. Without exception, each measurement requires calibration of the measuring device. Laser reflection, diffraction, and turbidity measurements require calibration on the very process stream which they are intended to monitor. Process upsets, feedstock changes, or even normal process changes under batch processing, may be manifested by changing optical properties of the process stream, which would invalidate the calibration of these instruments. Depending upon the application, the sensor output for feedback control could cause catastrophic results.

Measurements of photon migration

Measurements of photon migration differ from those described earlier in that they monitor the *time-dependent propagation characteristics* of multiply scattered light rather than the *amount of detected light*. Consequently, photon migration offers the following advantages for on-line measurement of PSD, CSD, or DPSD:

- Measurements are based on the "time-of-flight" of multiply scattered light as it consecutively scatters from particle to particle due to refractive-index mismatch between the particle or dispersed phase and the suspending fluid. Unlike other optical techniques, there is no calibration required for timing photon arrivals at a detector. Consequently, photon-migration techniques are "self-calibrating."
- Time-dependent measurements of photon migration provide prediction of isotropic scattering *and* absorption coefficients separately. Consequently, wavelength-dependent absorbances do not distort scattering measurements, thereby enabling accurate solution of the inverse problem for prediction of PSD and volume fraction, ϕ. Unlike turbidity measurements, wavelength-dependent absorbance changes are automatically accounted for and do not erroneously enter into the inverse solution for PSD and ϕ. In addition, since absorption spectra are simultaneously obtained, determination of stream composition may be possible.
- Since reemitted photons travel significant depths into a random medium, the measurement is reflective of PSD and volume fraction *within* the process stream and is less influenced by the partitioning of particles due to hydrodynamic wall effects.

As with all measurements, there are limitations to using photon migration techniques for on-line measurements of PSD and volume fraction determination:

- The concentration of particulates must be high enough so that multiple scattering occurs. This entails that the mean free-scattering path a photon travels between particles must be 100-fold smaller than the mean free path a photon travels before it is extinguished by absorption. In other words the isotropic scattering coefficient, $(1-g)\mu_s$, must be greater than the absorption coefficient, μ_a. In addition, the refractive indices of the dispersed and continuous phases must exist and be known *a priori*.
- The inversion algorithm used to reconstruct PSD and volume fraction from photon-migration measurements is similar to turbidity measurements in that it assumes that particles act as noninteracting, spherical scatterers.
- Depending upon the system employed, the form of the size distribution function (such as Gaussian, log-normal) can be employed to improve the reconstruction effort. While we report reconstructions assuming a Gaussian-like distribution of latex particle sizes, reconstructions can also be performed assuming an arbitrary but unimodal size distribution (Jiang et al., 1996b).

In the following, the theory behind frequency-domain photon migration for particle sizing in concentrated suspensions is described. Secondly, experimental measurements of frequency-domain photon migration using 15 or less wavelengths and their use to obtain a numerical solution to the inverse problem of reconstructing PSD and volume fraction are presented for three concentrated polydisperse latex suspensions. As discussed below, measurements were not referenced or calibrated using a reflectance or external standard. The agreement with DLS and exclusion chromatography results suggests the use of photon-migration techniques for on-line characterization or particles from 0.1 μm to 10 μm us-

Theory of Frequency-Domain Photon Migration

The techniques of photon migration have evolved from biomedical optical spectroscopy and imaging whereby multiply scattered near-infrared light is used to provide biodiagnostic information on tissue absorption and scattering (for reviews, see Chance et al., 1988; Sevick et al., 1991; Wilson et al., 1992). In this application, we employ frequency-domain measurements of photon migration to provide multiwavelength measurements of isotropic scattering on a suspension of noninteracting spheres for prediction of PSD and volume fraction from an efficient inverse algorithm. Frequency-domain measurements of photon migration depend on launching light whose intensity is sinusoidally modulated at MHz frequencies into a highly scattering process stream and monitoring the phase-shift, θ, and amplitude modulation, M, relative to the incident light (see Figure 2).

The propagation of light through random media can be described by the radiative transport equation (Duderstadt and Hamilton, 1976). Under conditions of multiple scattering (when the mean free-scattering path is significantly smaller than a mean free-absorption path), the time-dependent light

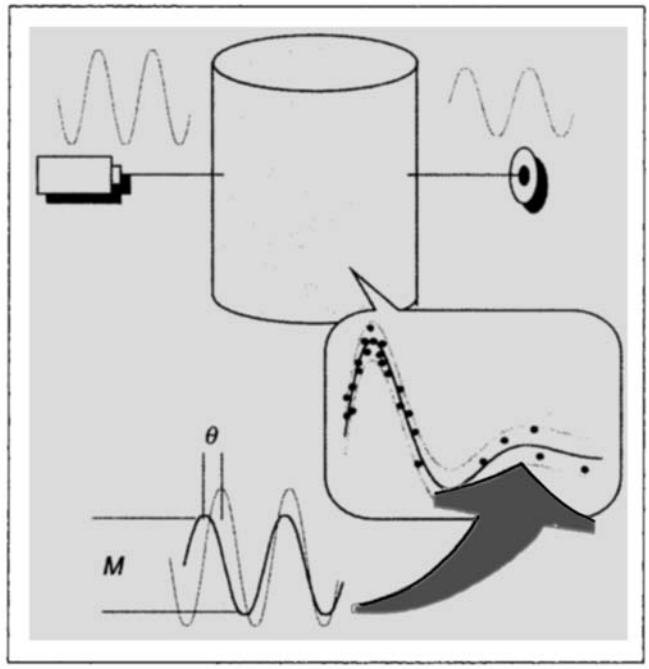

Figure 2. Frequency-domain photon-migration measurements.

Here, incident-intensity-modulated light is launched into a multiply scattering medium and the phase-shift and amplitude modulation of the reemitted wave is monitored.

propagation can be accurately modeled by a diffusion equation (Ishimaru, 1976; Chandrasekhar, 1960) written here in frequency space (Haskell et al., 1994):

$$-D(\lambda)\nabla^2\Phi(\mathbf{r},\omega)+\frac{i\omega}{c_n(\lambda)}\Phi(\mathbf{r},\omega)+\mu_a(\lambda)\Phi(\mathbf{r},\omega)=\delta(\mathbf{r}-\mathbf{r}_s)m, \quad (3)$$

where $\Phi(\mathbf{r},\omega)$ is the fluence of photons at position $\mathbf{r}$ associated with a propagating "photon density wave" modulated at frequency, ω; c_n is the speed of light through the medium; m is the depth of sinusoidal modulation of the source located at position $\mathbf{r}_s$; $\mu_a(\lambda)$ is the wavelength-dependent absorption coefficient that is equal to $\Sigma\,\epsilon[C]$, the sum of the product of extinction coefficients, ϵ and concentration $[C]$ for all light-absorbing constituents present; and $D(\lambda)$ is an "optical diffusion coefficient" that is given by

$$D(\lambda)=\frac{1}{3[\mu_a(\lambda)+(1-g)\mu_s(\lambda)]}. \quad (4)$$

The term $(1-g)\mu_s$ is the isotropic scattering coefficient that arises from multiple scattering and is dependent upon the particle-size distribution, $f(x)$, and the total volume fraction, ϕ:

$$(1-g)\mu_s(\lambda)=\mu_s'(\lambda)=\int_0^\infty \frac{3Q_{\text{scat}}(x,n,\lambda)[1-g(x,n,\lambda)]}{2x}\phi f(x)\,dx, \quad (5)$$

where g is the mean cosine of the scattering angle from a single particle, and Q_{scat} is the scattering efficiency. Both quantities are computed using classic Mie theory (Bohren and Hoffman, 1983).

The real and imaginary parts of $\Phi(|\mathbf{r}_s-\mathbf{r}_d|,\omega)$ can be used to predict the measured phase-shift, θ, and amplitude modulation, M, measured at detector position, $\mathbf{r}_d$.

$$\theta(\mathbf{r}_d,\omega,\lambda)=\tan^{-1}\frac{\text{Im}\,\Phi(\mathbf{r}_d,\omega,\lambda)}{Re\,\Phi(\mathbf{r}_d,\omega,\lambda)} \quad (6)$$

and

$$M(\mathbf{r}_d,\omega,\lambda)=\sqrt{[\text{Im}\,\Phi(\mathbf{r}_d,\omega,\lambda)]^2+[Re\,\Phi(\mathbf{r}_d,\omega,\lambda)]^2}. \quad (7)$$

The solution to Eq. 3 can be obtained for reflectance or transillumination measurements on semi-infinite random media as well as for infinite geometries in which the source and detector are separated by distance $|\mathbf{r}_s-\mathbf{r}_d|$. For semi-infinite geometries, the zero fluence, partial current, and extrapolated boundary are boundary conditions that are approximations of Snell's law of reflections that occur at refractive index-mismatched boundaries of air and random media (Haskell et al., 1994). In actuality, each of these boundary conditions essentially predicts the same measurements of phase-shift and amplitude modulation for the concentrated random medium (Patterson et al., 1991a). For simplicity, the measurements conducted herein represent an infinite media with the source and fiber optic embedded within a well-stirred suspension of polydisperse latex. The solution to Eqs. 3 and 6 can be written under these conditions (Patterson et al., 1991b):

$$\theta(\mathbf{r}_d,\omega,\lambda)\approx -|\mathbf{r}_s-\mathbf{r}_d|\sqrt{\frac{3\mu_s'(\lambda)\left\{(\mu_a(\lambda)c_n)^2+\omega^2\right\}^{1/2}}{c_n}}\times\sin\left[\tan^{-1}\left\{\frac{\omega}{\mu_a(\lambda)c_n}\right\}\right]. \quad (8)$$

Measurement of phase-shift usually includes a contribution due to the electronics and photodetection. Upon conducting a relative phase-shift measurement at two or more consecutive detector positions, $\mathbf{r}_{d_1}$, $\mathbf{r}_{d_2}$, instrument phase-errors associated with electron transit do not need to be accounted for. The relative phase, θ_{rel}, can then be predicted from (Fishkin et al., 1995):

$$\theta_{\text{rel}}(\lambda)=|\theta(\mathbf{r}_{d_1})-\theta(\mathbf{r}_{d_2})|=|\mathbf{r}_{d_1}-\mathbf{r}_{d_2}|\left(\frac{c_n^2\mu_a^2(\lambda)+\omega^2}{c^2D^2(\lambda)}\right)\sin\left[\frac{1}{2}\tan^{-1}\left(\frac{\omega}{c\mu_a(\lambda)}\right)\right]. \quad (9)$$

Experimental Approach for Photon-Migration Measurements in Latex Suspensions

Experimental measurements of phase-shift, θ, and amplitude modulation, M, were conducted using the laboratory

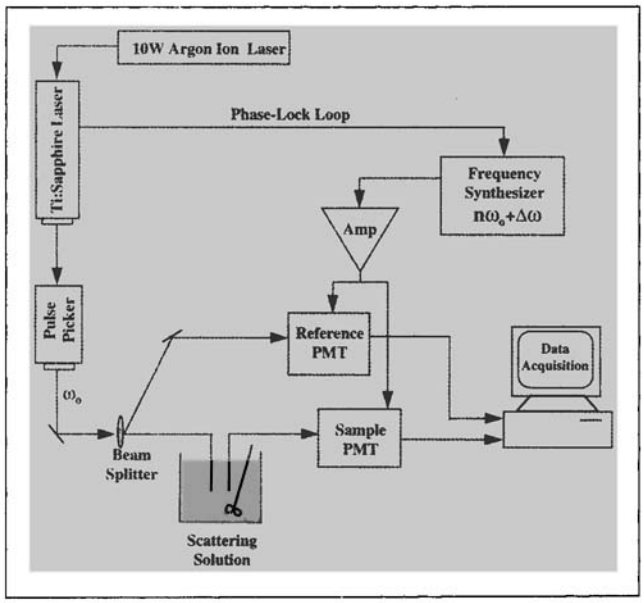

Figure 3. Frequency-domain instrumentation used to make measurements of phase-shift and amplitude demodulation.

laser apparatus system illustrated in Figure 3. While our instrumentation was bulky and complex for this feasibility study, a lamp-based system is currently under construction for use in a process analytic laboratory and ultimately for on-line use. However, in these measurements, the light source consisted of a picosecond pulsed titanium:sapphire laser (model 3950B Tsunami, Spectra Physics, MountainView, CA) pumped by a 10-W argon-ion laser (Beamlok 2060, Spectra Physics, CA). The Ti:sapphire laser produced an optical pulse train of equally spaced light pulses of 2 ps FWHM at a repetition rate of 80 MHz. The output beam was sent to an AOM crystal (model 3980, Spectra Physics) whose refractive index changed with applied RF to act as a shutter producing a pulse repetition rate of 4 MHz. Two sets of laser optics in the Ti:sapphire laser were used to provide wavelengths from 720 nm to 900 nm, and from 360 nm to 450 nm upon frequency doubling (model 3980, Spectra Physics). The average power exiting the AOM crystal and the frequency doubler was 50 mW and 10 mW, respectively. Depending on the wavelength desired, the pulsed-laser beam from the AOM or frequency doubler was sent to a glass-slide beam splitter that directed approximately 20% of the light to a reference photomultiplier tube (PMT) (Hamamatsu R928, Hamamatsu, Japan) via a 1,000 μm optical fiber (HCP-M1000T-08, Spectran, Avon, CT). The remaining light was directed to the scattering sample by another optical fiber that was held stationary and vertical in a clear acrylic cylindrical tank [9-in. (229-mm) OD $\times$ 8-in. (203-mm) height) filled with a latex suspension.

The light that propagated from the source fiber within the multiple scattering medium was collected by another fiber held in place within the tank. The detected light was then delivered to a second sample PMT via fiber-optic coupling. Fourier analysis of the 4-MHz pulse train delivered to the sample and reference PMTs yields a series of harmonic intensity-modulation frequencies at multiples of 4 MHz, which upon standard heterodyne detection techniques permit isolation of the individual intensity-modulated frequencies (Alcala et al., 1985). Heterodyning techniques were accomplished by gain modulating the PMTs at a harmonic of the laser repetition rate plus an offset cross-correlation frequency of 100 Hz. Gain modulation was accomplished using a commercial electronics package (ISS, Champaign, IL) and a -3-dBm RF signal from a frequency synthesizer (Marconi Instruments Signal Generator 2022A) amplified by a power amp (mode 1403LA, ENI, Rochester, NY). The resulting 100-Hz electronic signal from the heterodyned PMTs contained all information of phase-shift and amplitude modulation at the harmonic frequency of the pulsed-laser light delivered to the reference PMT and of the scattered light delivered to the sample PMT (Lakowicz, 1983). A standard data-acquisition module (ISS, Champaign, IL), originally developed for fluorescence lifetime measurements in nonscattering solutions was employed in a 486 IBM-compatible computer. By sweeping the RF signals at varying harmonics of the laser repetition rates, measurements of phase-shift, θ, and amplitude demodulation, M, relative to the incident light were conducted as a function of modulation frequency as well as wavelength. In order to obtain values of relative phase shift, θ_{rel}, measurements were conducted as the detecting fiber optic was moved with micrometer precision to distances of 1.0, 1.5 and 2.0 cm away from the source fiber optic. At each source-detector separation, measurements were conducted at 10 modulation frequencies ranging from 24 to 240 MHz. Relative phase shift between any two source-detector separations was determined by subtracting the phase shift measured at the farthest separation from that measured as a closer separation. By fitting experimentally measured relative phase shift at varying modulation frequencies to Eq. 9 using Levenberg–Maraquardt nonlinear least-squares regression, parameter estimates of μ_a and μ_s' were obtained.

Three polydisperse samples of polystyrene microsphere suspensions kindly provided by Dow Chemical were characterized using frequency-domain measurements of photon migration. The three polystyrene samples named, PP722, PP755, and PP788, had mean particle diameters of 0.57, 0.29, and 0.16 microns, respectively, as measured independently from DLS measurements (Microtrac Ultrafine Particle Analyzer, Honeywell, Leeds and Northrup, St. Petersburg, FL). Figure 4 illustrates the Gaussian particle-size distributions obtained from DLS, which agree well with size exclusion chromatography provided independently by Dow Chemical (data not shown for brevity). The concentration of solids for PP722, PP755, and PP788 were 47.95%, 52.74%, and 46.03% solids by volume, respectively, as determined through evaporation measurements. In order to neglect particle–particle interaction in the feasibility measurements presented herein, samples were diluted to 50 times their original concentration with deionized ultrafiltered water to obtain samples of approximately 1% solids by volume. These samples were multiply scattering, yet not too concentrated to cause interparticle interactions. For comparison, Fraden and Maret (1990) report reduction in isotropic scattering coefficients due to interparticle interactions of 0.46-μm polystyrene beads when the volume fractions exceed 15%. Work is ongoing to extend our analysis to increasingly concentrated suspensions. However, for the purposes of demonstrating particle sizing in multiply

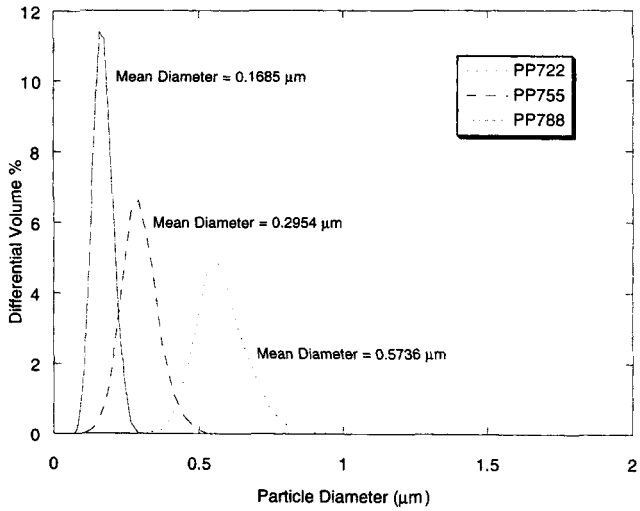

Figure 4. Particle-size distributions for all three scattering samples (Dow samples PP722, PP755, PP788) obtained by dynamic light-scattering analysis.

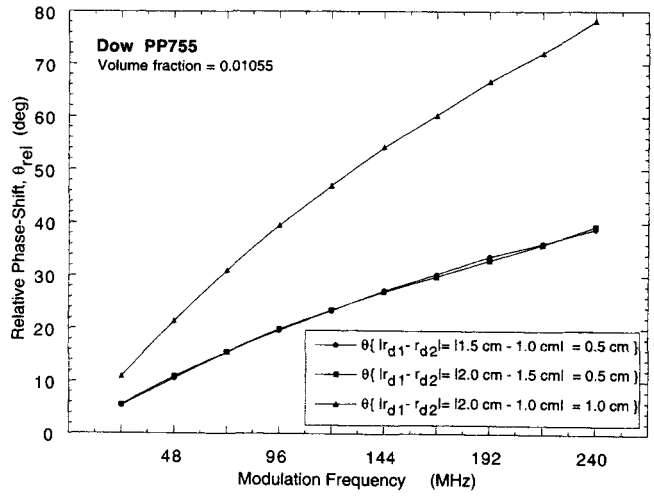

Figure 5. Experimental measurements (symbols) of relative phase shift, θ_{rel} (deg) vs. modulation frequency (MHz) for 1.055% diluted PP755 samples interrogated at 800 nm using source-detector separations of 2, 1.5 and 0.5 cm.

Relative phase-shift measurements of 0.5 and 1.0 are fit to Eq. 9 (solid line).

scattering systems, we restrict our analysis to solids volumes of 1%.

Experimental Results

Figure 5 illustrates the typical measurements of relative phase shift, θ_{rel}, on the 1.055% by volume PP755 sample as a function of modulation frequency at a wavelength of 800 nm. Measurements were conducted with source-detector separations, $|r_s - r_{d_i}|$, of 2.0, 1.5 and 1.0 cm. Consequently, relative phase shift was reported at relative source-detector separations of 1.0 and 0.5 cm. It is noteworthy that the two sets of phase-shift data recorded at detector separations of 0.5 cm fall upon one another, and the relative phase shift is twice as large at detector separations of 1.0 cm. This is consistent with Eq. 9, indicating that relative phase-shift changes vary with the magnitude of $|r_{d_1} - r_{d_2}|$. From the least-squares fit of Eq. 9, values of isotropic scattering and absorption coefficients were obtained from measurements conducted at 15 wavelengths between 360 and 800 nm. Table 1 lists the derived isotropic scattering coefficients as well as the predicted value of the isotropic scattering coefficient. The predicted values were obtained from Eq. 5 and employed Mie theory (Bohren and Hoffman, 1983) and experimental measurements of volume fraction and DLS size distribution. Figure 6 illustrates the experimentally obtained values of isotropic scattering as a function of wavelength (symbols) as well as the Mie theory prediction (solid line) for the PP788 sample. From the Table 1 and Figure 6, one can see that the measurements of isotropic scattering match Mie theory well. It is important to emphasize that these measurements were conducted without the use of any external reflectance or calibration standard. Table 2 provides the absorption coefficients obtained from the regression of Eq. 1. The absorption arises primarily from water. It is again worth mentioning that a suspending fluid with wavelength-dependent changes in absorption would influence scattering coefficients obtained from turbidity, angular scatterer, and laser reflection measurements. In photon-migration measurements, the influence of absorption is segregated from scattering without the need for calibration.

Inverse Algorithm for Determining $f(x)$ from Values of $\mu_s(\lambda)$

For a known particle-size distribution $f(x)$, Eq. 5 provides a straightforward way to calculate the isotropic scattering coefficient of the process stream from Mie theory. The results illustrated in Figure 6 validate Eq. 9 and the ability of photon-migration techniques to measure isotropic scattering coefficients. However, in order to solve for the particle-size distribution, $f(x)$, and the volume fraction, ϕ, from measurements of the isotropic scattering coefficients at multiple wavelengths, an inverse of Eq. 5, must be obtained. Our numerical inversion is based on a Newton-type iteration scheme to estimate $f(x)$ and ϕ through least-squares minimization of the function:

$$\chi^2 = \sum_{j=\lambda_1}^{\lambda_M} \left[(\mu_s')_j^o - (\mu_s')_j^c \right]^2, \tag{10}$$

where $(\mu_s')_j^o$ is the observed or measured isotropic scattering coefficient derived from values of relative phase-shift and $(\mu_s')_j^c$ is that computed from Eq. 5 for wavelengths, $j = \lambda_1, \lambda_2, \ldots, \lambda_M$, respectively.

In order to recover the particle-size distribution a method of updating $\phi f(x)$ is needed. Since $f(x)$ and ϕ can then be separated by the relation $\int_0^\infty \phi f(x)\, dx = \phi$, we choose to update the product, $\phi f(x)$, and consider the distribution to be equally divided into N bins representing $\phi f(x)_i$, $i = 1, N$. In order to update $\phi f(x)_i$ in each bin, the Jacobian matrix that describes the sensitivity of the isotropic scattering coefficient

Table 1. Experimentally Determined and Mie Theory Values of the Isotropic Scattering Coefficient for Three Latex Scattering Samples

Wavelength (nm)	PP722 μ_s' (cm^{-1}) Exp.	PP722 μ_s' (cm^{-1}) Mie	PP755 μ_s' (cm^{-1}) Exp.	PP755 μ_s' (cm^{-1}) Mie	PP788 μ_s' (cm^{-1}) Exp.	PP788 μ_s' (cm^{-1}) Mie
360	56.87	55.2	—	—	—	—
370	47.74	54.3	—	—	66.84	64.3
380	47.06	53.5	56.62	73.6	-	-
390	46.74	52.7	57.26	72.1	44.19	60.7
400	56.11	52.0	62.13	70.6	55.84	59.0
425	57.22	50.2	70.31	66.8	55.19	55.1
430	62.08	49.9	59.86	66.1	56.25	54.3
435	63.06	49.5	68.88	65.4	58.05	53.6
440	59.68	49.2	63.75	64.7	54.70	52.9
443	—	—	62.45	64.2	—	—
445	60.00	48.8	—	—	—	—
446	—	—	—	—	52.79	52.0
720	32.87	35.4	30.27	37.4	—	—
740	31.50	34.7	30.69	36.2	11.40	18.8
760	34.79	34.1	28.21	35.1	10.22	17.4
780	31.00	33.4	26.72	34.0	9.38	16.1
800	29.89	32.8	25.77	32.9	7.38	14.9
850	—	—	20.73	30.3	5.87	12.4

to changes in $\phi f(x)_i$ in each bin i and at each wavelength λ_j is computed. The Jacobian matrix is given by

$$\Im = \begin{bmatrix} \frac{\partial(\mu_s')^c_{\lambda_1}}{\partial[\phi f(x)]_1} & \frac{\partial(\mu_s')^c_{\lambda_1}}{\partial[\phi f(x)]_2} & \cdots & \frac{\partial(\mu_s')^c_{\lambda_1}}{\partial[\phi f(x)]_N} \\ \frac{\partial(\mu_s')^c_{\lambda_2}}{\partial[\phi f(x)]_1} & \frac{\partial(\mu_s')^c_{\lambda_2}}{\partial[\phi f(x)]_2} & \cdots & \frac{\partial(\mu_s')^c_{\lambda_2}}{\partial[\phi f(x)]_N} \\ \vdots & \vdots & \ddots & \vdots \\ \frac{\partial(\mu_s')^c_{\lambda_M}}{\partial[\phi f(x)]_1} & \frac{\partial(\mu_s')^c_{\lambda_M}}{\partial[\phi f(x)]_2} & \cdots & \frac{\partial(\mu_s')^c_{\lambda_M}}{\partial[\phi f(x)]_N} \end{bmatrix}, \tag{11}$$

and each element is computed numerically from solution of Eq. 5 with $\phi f(x)_i$ and $\phi f(x)_i + \Delta\phi f(x)_i$. The updates, $\Delta\phi f(x)_i$, resulting from the differences between measured and computed isotropic scattering coefficients can then be obtained from the resulting system of equations:

$$\Im^T \Im \Delta\zeta = \Im^T[(\mu_s')^o - (\mu_s')^c], \tag{12}$$

which is solved using Newton's method to obtain the vector $\Delta\zeta$ containing the updated values of $\phi f(x)$ across all bins, $i = 1, N$

$$\Delta\zeta = [\delta\{\phi f(x)\}_1, \delta\{\phi f(x)\}_2, \ldots, \delta\{\phi f(x)\}_N]^T. \tag{13}$$

The vectors, $(\mu_s')^o$ and $(\mu_s')^c$ contain the observed and computed values of isotropic scattering coefficients at the wavelengths of interest, $j = 1, M$:

$$[\mu_s'^o] = \left[(\mu_s')^o_{\lambda_1}, (\mu_s')^o_{\lambda_2}, \ldots, (\mu_s')^o_{\lambda_M}\right],$$

$$[\mu_s'^c] = \left[(\mu_s')^c_{\lambda_1}, (\mu_s')^c_{\lambda_2}, \ldots, (\mu_s')^c_{\lambda_M}\right]. \tag{14}$$

The preceding equations are suitable for an arbitrary particle-size distribution. However, for a real process stream, we usually have *a-priori* knowledge about the shape of the size distribution. For example, in many particulate process streams, the particle-size distributions are Gaussian or log-normal and can be described by only two parameters, the variance and mean, or a and b. In this work, we assume a Gaussian distribution:

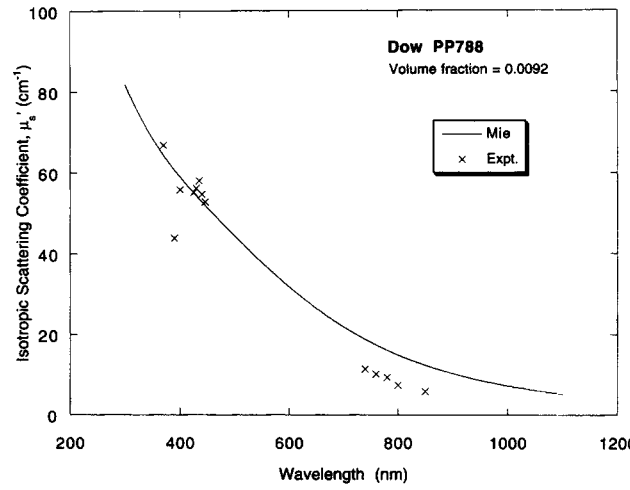

Figure 6. Isotropic scattering coefficient, μ_s' (cm^{-1}) vs. wavelength, λ (nm).

Derived from experimental measurements of phase shift (symbols) and computed from Mie theory, DLS and volume-fraction measurements (solid line). Data are reported for sample PP788 with a diluted volume fraction of 0.92%.

Table 2. Experimentally Determined Values for the Absorption Coefficient

Wavelength (nm)	μ_a (cm^{-1}) PP722	PP755	PP788
360	1.983E−03	—	—
370	3.223E−09	—	3.830E−04
380	1.713E−04	8.944E−05	—
390	5.229E−09	1.139E−03	2.122E−03
400	2.478E−03	6.742E−03	1.245E−02
425	4.870E−03	9.755E−03	9.726E−03
430	6.812E−03	5.937E−03	1.142E−02
435	7.207E−03	1.004E−02	1.331E−02
440	6.325E−03	6.468E−03	9.393E−03
443	—	5.172E−03	—
445	6.543E−03	—	—
446	—	—	8.949E−03
720	1.117E−02	1.039E−02	—
740	2.457E−02	2.652E−02	2.616E−02
760	3.072E−02	2.661E−02	2.785E−02
780	2.406E−02	2.504E−02	2.845E−02
800	2.190E−02	2.315E−02	1.977E−02
850	—	3.988E−02	3.780E−02

$$f(x) = \frac{1}{\sqrt{2\pi b}} \exp\left(-\frac{(x-a)^2}{2b}\right). \tag{15}$$

If we consider the volume fraction, ϕ, to be the third parameter, c, then we can further simplify the above Jacobian matrix $\Im$ to represent the sensitivity of isotropic scattering coefficients measured at wavelengths $j = 1,M$ upon the three parameters:

$$\Im = \begin{bmatrix} \frac{\partial(\mu_s')^c_{\lambda_1}}{\partial a} & \frac{\partial(\mu_s')^c_{\lambda_1}}{\partial b} & \frac{\partial(\mu_s')^c_{\lambda_1}}{\partial c} \\ \frac{\partial(\mu_s')^c_{\lambda_2}}{\partial a} & \frac{\partial(\mu_s')^c_{\lambda_2}}{\partial b} & \frac{\partial(\mu_s')^c_{\lambda_2}}{\partial c} \\ \vdots & \vdots & \vdots \\ \frac{\partial(\mu_s')^c_{\lambda_M}}{\partial a} & \frac{\partial(\mu_s')^c_{\lambda_M}}{\partial b} & \frac{\partial(\mu_s')^c_{\lambda_M}}{\partial c} \end{bmatrix}, \tag{16}$$

where again the elements of the Jacobian are numerically computed using Eq. 5. Hence $\Delta\zeta$ becomes the vector updating the three parameters, a, b, and c:

$$\Delta\zeta = [\delta a, \delta b, \delta c]^T. \tag{17}$$

Thus, the particle sizing task now becomes recovering the three parameters (a, b, and c) to describe $f(x)$ and ϕ. In work presented elsewhere, we have employed a Weibull distribution function that employs four parameters to successfully reconstruct ϕ and $f(x)$ of any arbitrary yet unimodal form, including Gaussian and log-normal distribution functions (Jiang et al., 1997). Extension to bimodal distributions would entail doubling the number of parameters. Reconstruction of multiple modes may also be possible.

The matrix $\Im^T\Im$ in Eq. 12 is basically ill-conditioned, and the typical way of dealing with this problem is to regularize or stabilize the decomposition of $\Im^T\Im$. While a number of regularization techniques exist, we have used the Maraquardt-type regularization scheme, which can be stated as

$$(\Im^T\Im + \alpha I)\Delta\zeta = \Im^T[(\mu_s')^o - (\mu_s')^c], \tag{18}$$

where I is the identity matrix and α may be a scalar or a diagonal matrix (Jiang et al., 1996). By adding a contribution to the diagonal terms in Eq. 18, we make $\Im^T\Im$ more diagonally dominant, which improves its invertibility. The parameter α is usually determined by trial and error.

In order to improve the inversion, we have also used a low-pass filter in our reconstruction algorithm. Once values of a, b, and c are updated, the size distribution is computed via Eq. 15, discretized, and numerically filtered by averaging over a window of width $N^*\Delta x$:

$$f(x_k)^{\text{new}} = (1-\zeta)f(x_k)^{\text{old}} + \frac{\zeta}{N^*}\sum_{l=k-(N^*/2)}^{l=k+(N^*/2)} f(x_l)^{\text{old}}, \tag{19}$$

where ζ is a factor between 0 and 1, and the summation is over the N^* particle sizes that surround the kth particle size. We have found that $\zeta = 0.35$ appears to give an optimal result for the cases studied in this work. In these initial reconstructions, we employed $N^* = 4$ with $\Delta x = 0.03$, 0.01, and 0.006 μm for PP722, PP755, and P788, respectively. We have found that the use of this low-pass filter enhanced the particle-size distribution recovery considerably by relaxing the requirement of a Gaussian size distribution. Obviously, the wider the distribution, the larger the filter width required for enhanced reconstruction. From the "filtered" $f(x)$, the isotropic scattering coefficient, $\mu_s'(\lambda)^c$, was computed and then used to update the Jacobian matrix described in Eq. 16 and to compute the updates to a,b,c using Eq. 18.

Inversion of Scattering Measurements to Produce PSDs

We have used the reconstruction algorithm described in Eqs. 12 and 15–17 to invert the isotropic scattering coefficient data listed in Table 1 to obtain $f(x)$ and ϕ for each of the three polydisperse suspensions. Our solution approach to the inverse problem found that the inversion results were not very sensitive to the choices of the initial guesses of the reconstructed parameters (a, b, and c), which were in the range between 30 and 100% relative to the exact parameters, depending, of course, on the noise of the optical property measurements. The particle-size distributions, $f(x)$, and volume fractions, ϕ, required five iterations until the function χ^2 reached a minimum value. Computational time for each inverse solution required a few seconds on a SunSparc 10 Workstation.

Figures 7 through 9 show experimentally reconstructed particle-size distributions for the three different suspensions, where the particle-size distributions determined by DLS have

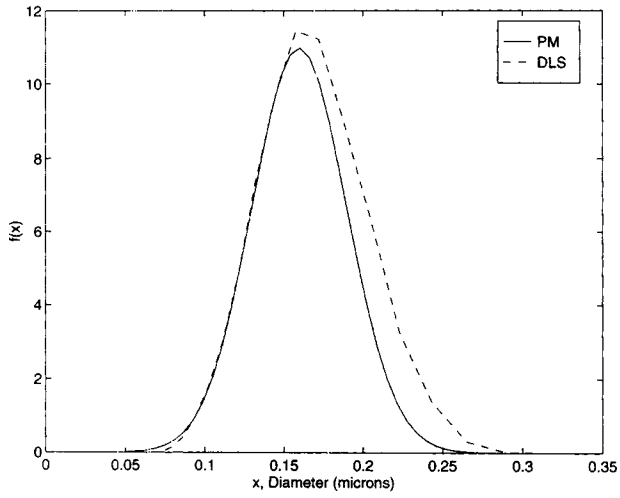

Figure 7. Particle-size distribution, $f(x)$ (dimensionless), as a function of diameter, x (μm), for PP788 sample as inverted from photon-migration measurements (solid line) and as measured from DLS (dashed line).

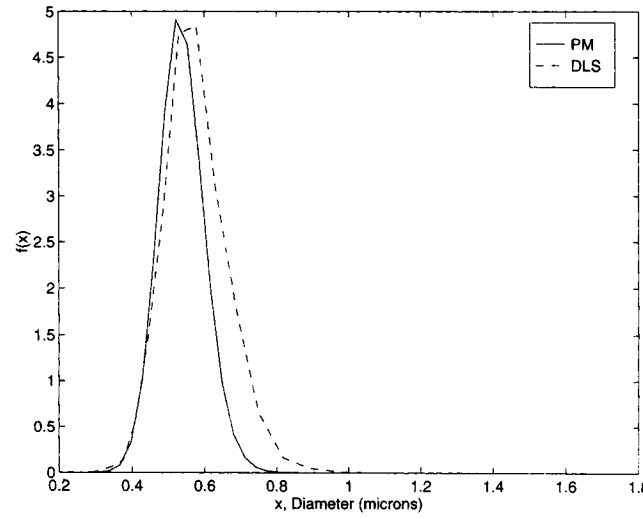

Figure 9. Particle-size distribution, $f(x)$ (dimensionless), as a function of diameter, x (μm), for PP722 sample as inverted from photon-migration measurements (solid line) and as measured from DLS (dashed line).

been included as dashed lines for comparison. As can be seen from the results, excellent agreement between our results and those by DLS has been reached. Since it is known that DLS causes an overprediction of particle-size distribution (Wang and Hallet, 1996), the errors between $f(x)$ from photon migration and DLS may be expected. Table 3 presents the results from the volume fraction calculations for the three different suspensions. Again, we see very good agreement between our results and those obtained by DLS.

Conclusion

In summary, we have presented the use of frequency-domain photon-migration measurements of isotropic scattering for robust solution of particle-size and volume-fraction measurements in concentrated suspensions. Typically, we were able to obtain excellent agreement with DLS measurements without needing to calibrate our measurement against any reflectance or external standard. In contrast to turbidity measurements, segregation of wavelength-dependent absorption effects from scattering measurements allow robust measurements for inversion. While our solution employed between 13 and 15 wavelength measurements, we have not yet tested the minimum number or choice of appropriate wavelengths required for a successful inverse solution. Work is currently in progress to assess the contribution of particle shielding on the scattering of electromagnetic waves in suspensions with $>1\%$ solids content. Optimizations of the inverse algorithms are also continuing in order to account for multimodal and arbitrarily shaped size distributions. Nonetheless, this current work demonstrates that the combination of a self-calibrating measurement and a robust inversion algorithm can produce readings to particle-size distribution and volume fractions in a matter of seconds. This work suggests the implementation of photon-migration measurements in particulate and dispersed phase-process monitoring, model validation, and control.

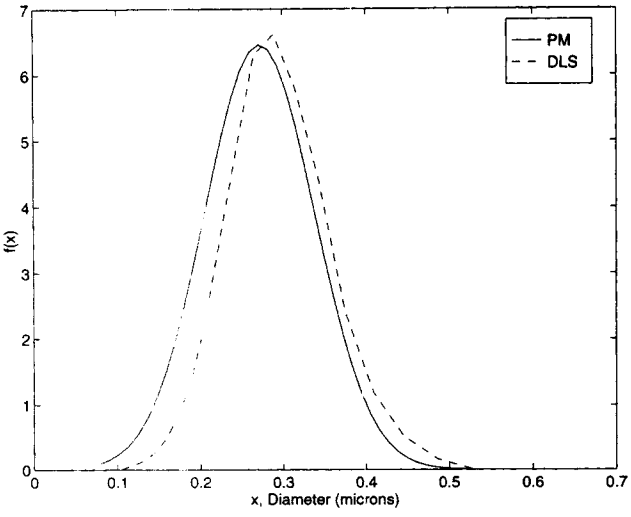

Figure 8. Particle-size distribution, $f(x)$ (dimensionless), as a function of diameter, x (μm), for PP755 sample as inverted from photon-migration measurements (solid line) and as measured from DLS (dashed line).

Acknowledgments

This work was funded in part by a National Science Foundation

Table 3. Solids Volume Fractions for Suspensions PP722, PP755, and PP788

	Values of ϕ from Photon Migration	Values of ϕ from DLS
PP722	0.76	0.95
PP755	1.32	1.53
PP788	0.57	0.63

Young Investigator Award (BES-9496239), the National Institutes of Health Research Career Development Award (K04-CA68374), DuPont 1995–1996 Educational Aid Program, the Purdue I/UCRC for Industrial Pharmacy, and the University of Tennessee Measurement and Control Engineering Center. The authors acknowledge the generous gift of polystyrene from Charles McDonald of Dow Chemical; the support and encouragement of Terry Redmond, Michael Chouinard, Gerald Lee, and Mohsen Khalili of Dupont; and Arlene Garrison of the University of Tennessee. We also acknowledge the helpful comments by Dilip Paithankar, Christina Hutchinson, and Steve Richter.

Literature Cited

Alcala, J. R., E. Gratton, and D. M. Jameson, "A Multifrequency Phase Fluorimeter Using the Harmonic Content of a Mode-locked Laser," *Anal. Instrum.*, **14**, 225 (1985).

Allen, T., *Particle Size Measurement*, 4th ed., Chapman & Hall, New York (1990).

Bohren, G. F., and D. R. Hoffman, *Absorption and Scattering of Light by Small Particles*, Wiley, New York (1983).

Chance, B., J. Leigh, H. Miyake, D. Smith, S. Nioka, R. Greenfeld, M. Finlander, K. Kaufman, M. Levy, M. Young, P. Cohen, H. Yoshioka, and R. Boretsky, "Comparison of Time-resolved and Unresolved Measurements of Deoxyhemoglobin in Brain," *Proc. Natl. Acad. Sci. USA*, **85**, 4971 (1988).

Chandrasekhar, S., *Radiative Transfer*, Oxford University Press, New York (1960).

Dimitratos, J., G. Elicabe, and C. Georgakis, "Control of Emulsion Polymerization Reactors," *AIChE J.*, **40**, 1993 (1994).

Duderstadt, J. J., and L. J. Hamilton, *Nuclear Reactor Analysis*, Wiley, New York (1976).

Elicabe, G. E., and L. H. Garcia-Rubio, "Latex Particle Size Distribution from Turbidimetric Measurements," *Polymer Characterization*, C. Carver and T. Provder, eds., ACS Adv. in Chemistry Ser. (1990).

Farrell, R. J., and Y.-C. Tsai, "Nonlinear Controller for Batch Crystallization: Development and Experimental Demonstration," *AIChE J.*, **41**, 2318 (1995).

Fishkin, J. B., P. T. C. So, A. E. Cerussi, S. Fantini, M. A. Franceschini, and E. Gratton, "Frequency-domain Method for Measuring Spectral Properties in Multiple Scattering Media: Methemoglobin Absorption Spectrum in a Tissue like Phantom," *Appl. Opt.*, **34**, 1143 (1995).

Fraden, S., and G. Maret, "Multiple Light Scattering from Concentrated, Interacting Suspensions," *Phys. Rev. Lett.*, **65**, 512 (1990).

Haskell, R. C., L. O. Svaasand, T.-T. Tsay, T.-C. Feng, M. S. McAdams, and B. J. Tromberg, "Boundary Conditions for the Diffusion Equation in Radiative Transfer," *J. Opt. Soc. Amer. A*, **11**, 2727 (1994).

Ishimaru, A., *Wave Propagation and Scattering in Random Media*, Academic Press, New York (1976).

Jager, J., J. M. Krammer, E. J. de Jong, S. de Wolf, O. H. Bosgra, A. Boxman, H. G. Merkus, and B. Scarlett, "Control of Industrial Crystallizers," *Powder Technol.*, **69**, 11 (1992).

Jiang, H., K. Paulsen, U. Osterberg, B. Pogue, and M. Patterson, "Optical Image Reconstruction Using Frequency-Domain Data: Simulations and Experiments," *J. Opt. Soc. Amer. A*, **13**, 253 (1996).

Jiang, H., J. Pierce, J. Kao, and E. M. Sevick-Muraca, "Measurement of Particle Size Distribution and Volume Fraction in Concentrated Suspensions Using Photon Migration Techniques," *Appl. Opt.*, in press (1997).

Kourti, T., J. F. MacGregor, A. E. Hamielec, D. F. Nicoli, and V. B. Elings, "On-line Particle Size Determination During Latex Production Using Dynamic Light Scattering," *Polymer Characterization*, C. Carver and T. Provder, eds., ACS Adv. in Chemistry Ser. (1990).

Lakowicz, J. R., *Principles of Fluorescence Spectroscopy*, Plenum Press, New York (1983).

Monnier, O., J.-P. Klein, C. Hoff, and B. Ratsimba, "Particle Size Determination by Laser Reflection: Methodology and Problems," *Part. Part. Syst. Charact.*, **13**, 10 (1996).

Patterson, M. S., S. J. Madsen, J. D. Moulton, and B. Wilson, "Diffusion Equation Representation of Photon Migration in Tissue," *IEEE MTT-S Int. Microwave Symp. Digest*, **2**, 905 (1991a).

Patterson, M. S., J. D. Moulton, B. C. Wilson, and B. Chance, "Applications of Time-Resolved Light Scattering Measurements Using Phase Modulation Spectroscopy," *Proc. SPIE, Int. Soc. Opt. Eng.*, **1203**, 62 (1991b).

Rawlings, J. B., S. M. Miller, and W. R. Witkowski, "Model Identification and Control of Solution Crystallization Processes," *Ind. Eng. Chem. Res.*, **32**, 1275 (1993).

Sevick, E. M., B. Chance, J. Leigh, S. Nioka, and M. Maris, "Quantitation of Time- and Frequency-Resolved Optical Spectra for the Determination of Tissue Oxygenation," *Anal. Biochem.*, **195**, 330 (1991).

Silebi, C. A., and J. G. Dos Ramos, "Theoretical and Experimental Study of Capillary Hydrodynamic Fractionation," *Polymeric Mat. Sci. and Eng., Proc. of ACS Div. of Polymeric Mat. Sci. and Eng.*, **61**, 85 (1989).

Sparks, R. G., and C. L. Dobbs, "The Use of Laser Backscatter Instrumentation for On-Line Measurement of the Particle Size Distribution of Emulsions," *Part. Part. Syst. Charact.*, **10**, 279 (1993).

Thomas, J. C., and V. Dimonie, "Fiber Optic Dynamic Light Scattering from Concentrated Dispersions. 3: Particle Sizing in Concentrates," *Appl. Opt.*, **29**, 5332 (1990).

Van de Hulst, H., *Light Scattering by Small Particles*, Dover, New York (1983).

Vavra, J., J. Antalik, and M. Liska, "Application of Regression Analysis in Spectroturbidity Size-characterization Methods," *Part. Part. Syst. Charact.*, **12**, 38 (1995).

Wang, P.-H., G. S. Kent, M. P. McCormick, L. W. Thomason, and G. K. Yue, "Retrieval Analysis of Aerosol-Size Distribution with Simulated Extinction Measurements at SAGE III Wavelengths," *Appl. Opt.*, **35**, 433 (1996).

Wang, J., and F. R. Hallet, "Spherical Particle Size Determination by Analytical Inversion of the UV-Visible-NIR Extinction Spectrum," *Appl. Opt.*, **35**, 193 (1996).

Wilson, B. C., E. M. Sevick, M. S. Patterson, and B. Chance, "Time-dependent Optical Spectroscopy and Imaging for Biomedical Applications," *Proc. IEEE*, **80**, 918 (1992).

Manuscript received July 22, 1996, and revision received Oct. 3, 1996.